Journal of Power Sources 268 (2014) 315–325

Contents lists available at ScienceDirect

Journal of Power Sources

journal homepage: www.elsevier.com/locate/jpowsour

The impact of calendar aging on the thermal stability of a $LiMn_2O_4$–$Li(Ni_{1/3}Mn_{1/3}Co_{1/3})O_2$/graphite lithium-ion cell

Patrick Röder [a, *], Barbara Stiaszny [a], Jörg C. Ziegler [a], Nilüfer Baba [a], Paul Lagaly [a], Hans-Dieter Wiemhöfer [b]

[a] Robert Bosch GmbH, Corporate Sector Research and Advance Engineering, Postfach 10 60 50, 70049 Stuttgart, Germany
[b] Institute of Inorganic and Analytical Chemistry, University of Münster, Corrensstr. 28/30, 48149 Münster, Germany

HIGHLIGHTS

- The aged cells show changes in their thermal behavior on cell and material level.
- Main reason for aging is loss of cycleable lithium.
- A more pronounced SEI after aging leads to a lower onset-temperature.
- At the same time the released energy of the anode-electrolyte reaction is increased.
- The impact of the cathode potential during aging on the thermal stability was investigated.

ARTICLE INFO

Article history:
Received 9 April 2014
Received in revised form
20 May 2014
Accepted 8 June 2014
Available online 15 June 2014

Keywords:
Aging
$LiMn_2O_4$
NMC
Safety
ARC
DSC

ABSTRACT

Aging of lithium-ion cells is an inevitable phenomenon limiting the lifetime. Undesirable side reactions during cycle or calendar aging may affect the performance of all components of the lithium-ion cell. This results in a decreased capacity and an increase in the overall cell impedance. Based on electrochemical and physical characterization methods, the aging behavior during calendar aging of a 18650-cell, containing a blend of $LiMn_2O_4$ and $Li(Ni_{1/3}Mn_{1/3}Co_{1/3})O_2$ (NMC) as cathode material and graphite as anode material was systematically investigated. To understand how the safety behavior of a lithium-ion cell changes with aging, accelerating rate calorimetry (ARC) and differential scanning calorimetry (DSC) were applied. With these methods the thermal stability behavior of the complete lithium-ion cell and its respective cathode and anode material were investigated.

The focus of this work was it to generate first cause–effect relations between the aging under one exemplary aging condition and the thermal stability of a lithium-ion battery both on cell and material level.

1. Introduction

The high power and energy density of lithium-ion cells have made them one of the most attractive energy storage systems. Nowadays they are widely used in portable electronic devices like laptops, cameras and mobile phones. In the past few years lithium-ion cells have drawn much attention for their operation in automotive applications like hybrid vehicles (HEV), plug-in hybrid electric vehicles (PHEV) and full electric vehicles (EV). These applications require long cycle and calendar life, typically up to 15 years, low cost, high power and also safe operation throughout the whole lifetime, i.e. the safety of the cell should not be negatively influenced by the aging of the lithium-ion cell.

Although there is a large variety of possible materials combinations for electrodes in lithium-ion cells, combining high cycle stability and high specific capacity reduces the choices to a palmful. Promising candidates for cathodes are layered oxides like $Li(Ni_{1/3}Co_{1/3}Mn_{1/3})O_2$ which exhibits high specific capacity [1], but discharge at high rates is limited. To increase safety and especially rate capability in the cell, $LiMn_2O_4$ is added to the cathode because it exhibits the fast kinetics that is necessary for high power applications [1,2]. Substitution of Mn for Ni or Co in corresponding cathode materials is also favored since this reduces the cell's cost, although the specific capacity of these mixed metal oxides is lower.

* Corresponding author. Tel.: +49 (0)7117583344.
E-mail address: patrick.roeder@de.bosch.com (P. Röder).

http://dx.doi.org/10.1016/j.jpowsour.2014.06.040
0378-7753/

$LiMn_2O_4$, in particular, suffers from rapid degradation especially at elevated temperatures due to manganese dissolution [1]. The best anode material considering both specific capacity and cycleability is graphite [2].

It is commonly known that the lifetime of lithium-ion cells is limited by unwanted side reactions [3]. These side reactions may affect all parts of a cell including the electrolyte, the active material, binder, conducting agents, current collectors and the separator which results in capacity decrease and/or increase of the overall cell impedance [3–5]. These side reactions may also influence the safety of the cells.

Regarding the safety of lithium-ion cells, concerns about the thermal behavior of the oxide-based cathode materials still exist since oxygen release from the cathode material at higher temperatures can lead to a hazardous combustion reaction driving the flammable alkylcarbonate-based solvent of the electrolyte into fire or explosion. The thermal behavior of complete lithium-ion cells is primarily dominated by the used electrode materials, in particular the cathode materials and their thermal decomposition behavior as well as the reaction behavior with the organic based electrolyte. Using C80 microcalorimetry, differential scanning calorimetry (DSC) or accelerating rate calorimetry (ARC), the thermal stability of various lithium-ion electrode materials in contact with salt-free solvent and electrolyte was already investigated by many researcher groups, e.g. [6–9]. The impact of different influence parameters, like the state of charge (SOC), was thereby investigated. Also complete new cells were investigated in literature [10–12]. Roth and Doughty [13] investigated the thermal stability of aged cells ($Li(Ni_{0.8}Co_{0.15}Al_{0.05})O_2$/Graphite) both on the complete lithium-ion cell and its electrode materials in contact with electrolyte. To the best of our knowledge up to now there are no further detailed investigations about the impact of aging on the thermal stability of lithium-ion cells. Commonly, only fresh cells and their electrode materials are investigated.

In this work calendar aged lithium-ion cells were investigated by ARC, DSC and various electroanalytical methods. The investigations were performed both on the complete lithium-ion cell and separately on its cathode and anode material, respectively.

This work aims at a detailed thermal and electrochemical coupled study of new and aged lithium-ion cells under one exemplary aging condition to generate first possible cause–effect relations between aging and the thermal stability both on cell and material level.

Therefore, in the first section of this work the main aging phenomena were extracted based on the physical and electroanalytical methods. In the second section the impact of these aging effects on the thermal behavior of the cell and its respective active materials was investigated based on ARC and DSC.

2. Experimental

2.1. Cell-type

Commercial 18650 lithium-ion cells containing a blend of $Li(Ni_{1/3}Mn_{1/3}Co_{1/3})O_2$ and $LiMn_2O_4$ (3:1, w/w) as cathode material and graphite as anode material with an initial capacity of 2 Ah have been used in this work. In the following, this cell-type will be labeled as cell "A".

For a second experiment, where aging mechanisms are not in the focus but only the thermal behavior of the cathode studied by ARC, a pouch cell containing also $Li(Ni_{1/3}Mn_{1/3}Co_{1/3})O_2$ and $LiMn_2O_4$ (4:1, w/w) as cathode material and hard carbon as anode material with an initial capacity of 2 Ah has also been used (see Section 3.4.3). This cell-type is labeled as cell "B".

Table 1
Fitted resistance values of new and aged cell A.

Cell	R_{el} [Ω]	R_{SEI} [Ω]	R_{Anode} [Ω]	$R_{Cathode}$ [Ω]
New cell A	0.040	0.026	0.081	0.065
Aged cell A	0.058	0.069	0.076	0.051

2.2. Cell storage

Four identical cells are stored at a voltage of 4.2 V (SOC100) at 60 °C. The cells are stored at open circuit potential, thus no trickle charge is applied and the cell is allowed to change its voltage by self-discharge between two characterization segments. This aging procedure was applied both for cell A and B.

During storage the power, the 1C and C/5 capacity is monitored every 6 weeks.

The power and inner resistance was determined (only cell A) with 12 A discharge pulses, which were applied for 10 s at different SOCs (between SOC100 and SOC10 in steps of 10% SOC). The voltage and current were taken just prior to the pulse and at the end of the pulse after 10 s to calculate the inner resistance by the following Equation (1).

$$R_{DC} = \frac{U_{10s} - U_{0s}}{I_{10s} - I_{0s}} = \frac{\Delta U}{\Delta I} \quad (1)$$

The specific power in W kg^{-1} was calculated by multiplication of voltage and current at the end of the pulse after 10 s divided by the mass of the cell as shown in Equation (2).

$$P = \frac{U_{10s} \cdot I_{10s}}{m_{Cell}} \quad (2)$$

The capacity was determined at a discharge rate of 1C and C/5. The cells were discharged to a voltage of 2.75 V as recommended by the cell supplier.

After the power and capacity test, the standard charging procedure recommended by the manufacturer was applied. Cells were charged at a constant current rate of 2 A from 2.75 V to 4.2 V and subsequently the potential was held constant at 4.2 V until the total charging time exceeded 3 h.

The characterization was carried out with a BaSyTec Cell Cycler at room temperature.

2.3. Laboratory test cells

For post mortem analysis and characterization, the cells were opened in an argon-filled glovebox. To prevent (internal) short circuits during the whole disassembling process ceramic opening instruments were used. Electrode disks with a diameter of 18 mm were punched out of the cell roll for use in so called "EL-Cells", which are commercially available test cells [14]. Before using the electrode sheets the coating had to be removed on one side of the current collector in order to get electrical contact. Particularly with aged electrodes the coating easily flakes off or sticks to the separator, making it a challenge to gain fully coated electrode sheets. After removing the coating the sheet was washed in dimethyl carbonate and dried at room temperature to remove residues from the electrolyte.

For all laboratory test cells a glass fiber separator with a diameter of 18 mm and a thickness of 1.55 mm served as the electrolyte reservoir. 1 M $LiPF_6$ in a mixture of ethylene carbonate (EC) and dimethyl carbonate (DMC) at a ratio of 1:1 (v/v%) was used as the electrolyte in the laboratory test cells.

In total two types of laboratory test cells were prepared.

- *Half cells* having anode or cathode as working electrode and metallic lithium as counter and reference electrode (e.g. data shown in Fig. 4 and Table 2).
- *Full cells* with cathode and anode plus metallic lithium as reference electrode to monitor the potentials of anode and cathode during cycling (e.g. data shown in Fig. 5)

2.4. Electrochemical investigation

Slow-scan cyclic voltammetry was carried out at cathode half cells with a scanning rate of 5 μV s^{-1} to investigate the redox voltages and peak heights of the new and aged electrodes of cell A.

Full cells with reference electrodes were assembled to measure the potentials of the anode and cathode during cycling of new and aged cells. In these experiments the potentials of anode and cathode of cell A were monitored against the lithium reference electrode while cycling the cell between 4.2 V and 2.75 V.

Low rate capacity tests were performed on the new and aged anode as well as the cathode within half cells. For the new and aged anode the half cell was cycled with a C/25 rate between 1 V and 5 mV followed by a 3 h CV step. The same cycling procedure was used for the cathode between 3.3 V and 4.3 V.

Electrochemical impedance spectroscopy was carried out using a Gamry Instruments Potentiostat PCI4G300-51021 (Series-G300). Full cells were discharged to SOC10 at a rate of C/5 and kept at OCV for four hours before the measurement started. The impedance of cells was measured in hybrid mode in the frequency range between 10^5 Hz and 2 mHz with a perturbation voltage of 1 mV at temperatures of 23 °C, 0 °C and −10 °C. Calendar aged cells are characterized after 24 and 36 weeks of storage. Temperature control was achieved in a climate chamber.

2.5. Physical – analytical investigation

Surface investigations were done by a Gemini Leo 1530 scanning electron microscope equipped with Oxford Instruments analytical tools. For surface pictures typically an acceleration voltage of 5 kV was used, whereas for EDS analysis 20 kV was selected.

As a reference state, a pristine cell A was fully characterized by the designated methods.

2.6. Thermal investigation

2.6.1. Sample preparation

The fully charged cell (SOC100, cell A and B) was transferred in an argon-filled glovebox and afterwards disassembled with ceramic instruments to prevent (internal) short circuits. The cathode material was scraped from the aluminium collector and rinsed with dimethyl carbonate (DMC) to remove the original electrolyte and additives from the surface of the electrode material and from accessible pores. Finally, the rinsed cathode material was dried under vacuum overnight to guarantee that all DMC was removed, before doing any ARC experiments. The anode material was not rinsed with DMC since the rinsing procedure would remove the organic components of the SEI [9].

Table 2
Low rate capacity (C/25) values of anode and cathode (new and aged cell A) vs. Li/Li^+.

vs. Li/Li^+	Capacity new [mAh]	Capacity aged [mAh]
Anode (cell A)	7.40	7.38
Cathode (cell A)	7.45	6.92

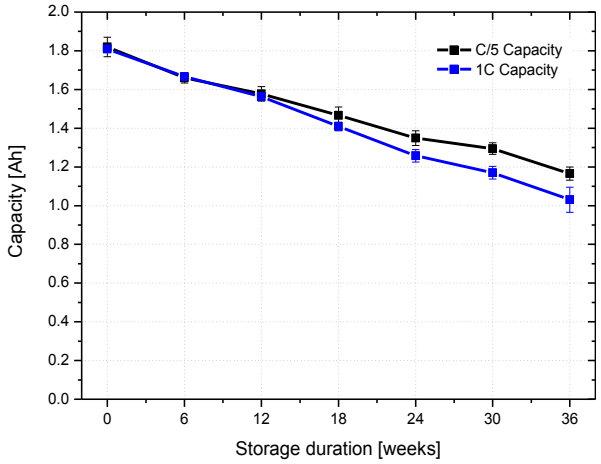

Fig. 1. Capacity decrease at 1C and C/5 discharge rate of cell A during calendar aging at 4.2 V (SOC100) and 60 °C. Error bars represent the standard deviation of four identical cells.

For all ARC and DSC experiments the reference electrolyte consisted of a solution of 1 M $LiPF_6$ in ethylene carbonate (EC) and dimethyl carbonate (DMC) with a ratio of 1:1 (v/v%).

2.6.2. Accelerating rate calorimetry (ARC)

All ARC experiments were carried out by an APTAC 254® from Netzsch Gerätebau GmbH (Germany).

The ARC samples, consisting of the prepared active material and the standard electrolyte, are placed into a titanium sample holder with a wall thickness of only 0.1 mm. Our sample holder guarantees a low thermal mass. The importance of calibration and the thermal mass of a sample holder to retain precise ARC measurements was discussed in [15]. A sample mass of 200 mg of the cathode material and 60 mg of the reference electrolyte were commonly used to carry out the ARC experiments. Due to the low density of the anode material, in this case, only 100 mg of the anode material and 50 mg electrolyte were used. Since the electrode material was obtained from commercial lithium-ion cells, the weight of the electrode powder includes both carbon and binder.

The whole preparation for an ARC experiment was carried out under argon atmosphere to prevent atmospheric influences (especially oxygen and water). First of all, the samples were heated up to a start temperature of 80 °C. A measurement commonly stopped at 350 °C or when the self heating rate of the sample rose beyond 40 K min^{-1}. In 5 K steps a heat-wait-search procedure (HWS) was applied with a waiting time of 15 min before searching for exothermal processes. If no exotherm was found, the temperature was increased with a heating rate of 5 K min^{-1}. The threshold for an exothermic process was set to a heating rate of 0.02 K min^{-1}. When the generated heat of our sample exceeded this threshold, the following exotherm was monitored under adiabatic conditions. Besides the detection of the temperature and the heating rate of our sample, we also recorded the pressure rise during an ARC measurement.

All boundary conditions as described above, such as heating rate or detection threshold were the same for the ARC measurements of the complete lithium-ion cells.

2.6.3. Differential scanning calorimetry (DSC)

All DSC measurements were performed with a Netzsch DSC 204 F1 Phönix from Netzsch Gerätebau GmbH (Germany).

The complete DSC preparation was also done under argon atmosphere to prevent atmospheric influences. We used a scan rate of 5 K min^{-1} to carry out the DSC measurements. The electrode material was investigated in presence of our reference electrolyte. For the sake of comparability, we tried to adjust a mass ratio of 1:1 (w/w) between the solid electrode material and the liquid electrolyte. In the following work, the respective mass ratios are indicated in the respective DSC – plots as C/E. The released heat can be calculated as integral of the DSC plot. In this work, the released heat for the cathode – electrolyte measurements were evaluated between 150 °C and 350 °C. Due to a larger exothermic domain, all the indicated heat values for the anode – electrolyte measurements were evaluated between 80 °C and 350 °C.

3. Results and discussion

3.1. Investigation during storage

During storage the capacity of four identical cells (cell A) was monitored at a discharge rate of 1C and C/5 as shown in Fig. 1.

It can be seen that the capacity of the cell A continuously decreases within 36 week from ~2 Ah to ~1 Ah. Furthermore the devolution of power and inner resistance at 10 different SOCs (SOC100 – SOC10) are plotted in Fig. 2. It is obvious that the power decreases with increasing storage duration, because the inner resistance of the cell increases continuously. At storage durations >12 weeks the C/5 and 1C discharge capacity, as shown in Fig. 1, start to drift apart which can be reasoned by an increased inner resistance. The power (P = U*I) is mainly determined by the inner resistance, but the capacity loss will cover a small part. The power is measured by 10 s pulses, where the capacity loss has a minor effect.

Fig. 3a shows the impedance spectra of the new and 36 weeks calendar aged cell A. Both spectra were taken at SOC10 and 0 °C. After aging at elevated temperatures, two obvious aging effects can be seen. The ohmic resistance of the calendar aged cell A (intersection of EIS curve with *x*-axis) remarkably increased as well as the overall cell impedance.

The spectra have been fitted with a reasonable electrical equivalent circuit as shown in Fig. 3b (a detailed discussion of the equivalent circuit as used here has been described in a previous paper [16]).

Table 1 shows the fitted resistance values of the new and aged cell A.

The serial resistance significantly increases during aging indicating a reduced ionic conductivity of the electrolyte possibly due to decomposition of the electrolyte. Another remarkable increase could be found for the SEI layer resistance. The SEI layer is built up of decomposition products of the electrolyte [17]. The charge transfer resistance of the anode is reduced in the aged state. This phenomenon was already seen from other cells in our previous paper [16] and could be assigned to an increased surface of the anode in the aged state, caused by particle cracks etc. The charge transfer resistance of the cathode is also reduced. This could be an effect of a significantly higher cathode potential in the aged state at SOC10 (see Fig. 5a). Since the cathode charge transfer resistance is highly dependent on the potential of the cathode (decreasing charge transfer resistance with increasing cathode potential), this can explain the fit data for the cathode charge transfer. This effect is described in detail in [16].

Finally, it can be seen that the total resistance of the cell increases both for the DC measurement in Fig. 2 and the impedance investigations in Fig. 3. The resistance in Fig. 2 contains the IR drop from the electrolyte and the hindered charge-transport into the particles. In AC measurement (impedance) the ohmic resistance increases coming from the electrolyte. Diffusion was not evaluated and R_{SEI} increases which equates to a hindered charge-transport process. This behavior leads finally to a reduced power performance accompanied with loss of cycleable lithium since the electrolyte is reduced at the anode during aging.

3.2. Electrochemical investigation of the aged cell

Table 2 shows the low rate capacities (C/25 rate) of the new and the aged anode as well as the cathode of the cell A measured in a half cell (vs. Li/Li^+) indicating the capacity loss due to loss of active material and and/or isolated particles in the electrode since a limitless lithium reservoir is present. The values show that the capacity loss in case of the cathode is around 7% and in case of the anode no significant loss of active material can be observed (around 0.5%).

To closer investigate the loss of active material at the cathode of cell A slow-scan cyclic voltammetry has been conducted, as shown in Fig. 4. The mass of active materials are same. The spikes in the CV measurements can be explained by the very small currents due to the low scan rates leading to a resolution limit of the used battery cycler. Reduced peak heights at the position of the NMC and the spinel can be observed. NMC appearing at ~3.7 V [18] shows a prominent decrease of its peak height corresponding to loss of active material by transition metal dissolution and/or isolated particles in the electrode. $LiMn_2O_4$ is active >3.8 V [16] (2 peaks) and shows a reduced peak height as well.

Detailed x-ray diffraction (XRD) investigations for nearly the same blend material can be found in [16] and [19] indicating the loss of transition metals.

However, the 7% loss of active material at the cathode and 0.5% at the anode cannot account for all the capacity losses seen in the

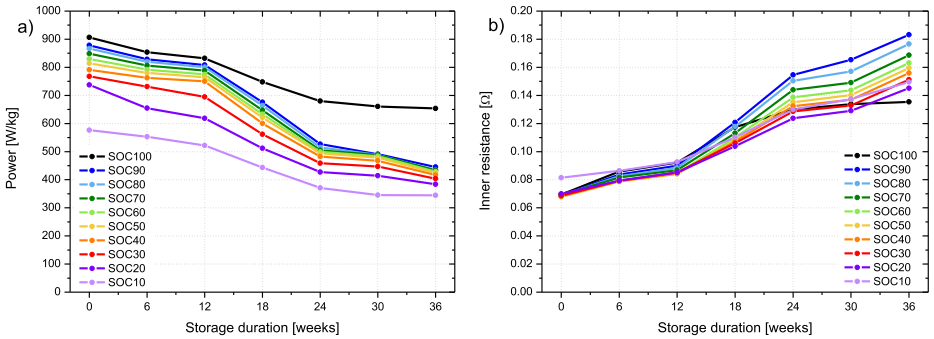

Fig. 2. a) Power and b) internal resistance evolution for different SOCs during calendar aging of cell A at 4.2 V and 60 °C. As a result of the increase of the internal resistance the power decreases.

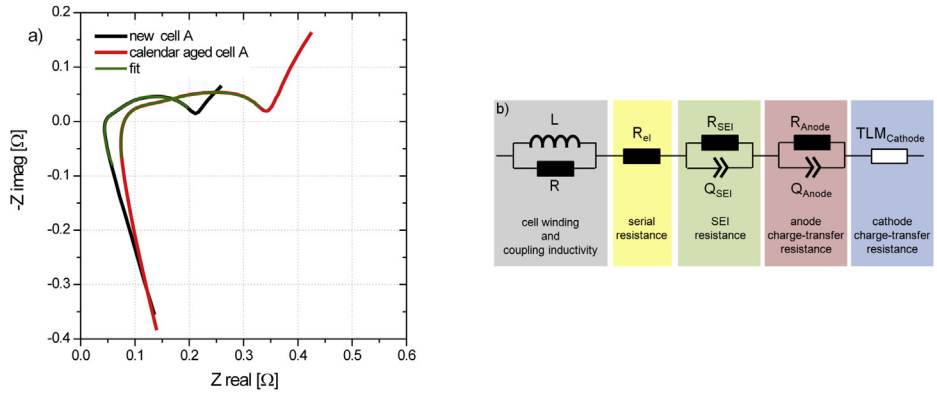

Fig. 3. Impedance spectra of new and calendar aged cell A in a) Nyquist and b) electrical equivalent circuit for fitting. All spectra are taken at SOC10 at 0 °C.

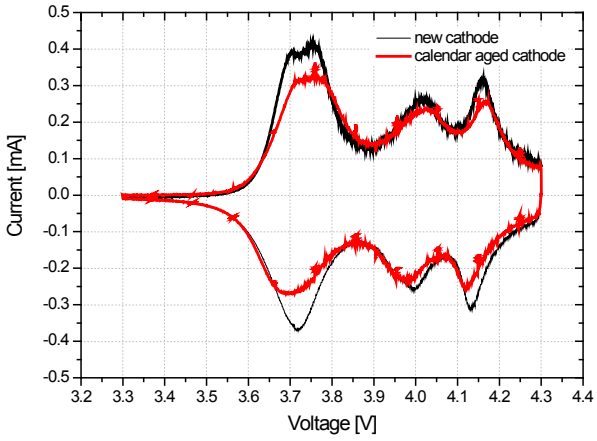

Fig. 4. Slow-scan cyclic voltammetry of the new and aged cathode of cell A with a scan rate of 5 $\mu V\ s^{-1}$.

complete cell A after 36 weeks of storage. This overall capacity loss of cell A, as shown in Fig. 1, is about 40% with a C/5 rate. Therefore further investigations are necessary.

With the help of a reference electrode the potential of anode and cathode can be monitored during cycling, which is important to investigate at which potentials the single electrodes run during cycling. An so called EL-Cell with anode and cathode + metallic lithium reference electrode was charged with C/25 to 4.2 V, followed by a 3 h CV step at 4.2 V. Fig. 5 a represents the potential curves of new (dashed lines) and aged (solid lines) electrodes of cell A within a full cell during charging. The corresponding discharge step with C/25 to 2.75 V is seen in Fig. 5b.

A reduction of the cell capacity is obvious as compared to the fresh cell, which results from the fact that the voltage level of the aged cathode, and thus the aged full cell, increases faster compared to the new cell. The rise of voltage due to a higher inner resistance is unlikely due to the low current rate of C/25 and the usage of fresh electrolyte. The cell voltage may rise during use, but the voltage curve should start at equal points in the discharged state.

The voltage curves of the new and aged anode run at exactly the same potential, but the lower plateau of the aged graphite vs. lithium curve is not used to full capacity as the dashed line shows it for new graphite vs. lithium. This graph shows that more than half of the graphite's lower plateau is not utilized in the cell's aged condition and corresponds to a capacity loss of more than 30%.compared to only 7% for the cathode material or 0.5% for the anode material, shown in Table 2. Hence, this phenomenon can be only associated to a minor extent by loss of positive active material and mostly by loss of cycleable lithium. In case of this full cell test a limited lithium reservoir is applied in contrast to the low rate capacity test (half cells), shown in Table 2. During charging and storage at high voltages lithium is irreversibly consumed in side reactions like SEI layer growth on the anode. This mostly is the reason why the cathode cannot be fully lithiated during discharge and is therefore at a more positive potential in the discharged state. As already mentioned structural changes (e.g. loss of active material [16,19]) influences the lithiation degree only to a minor extend. Consequently the anode is also at a more positive potential in the

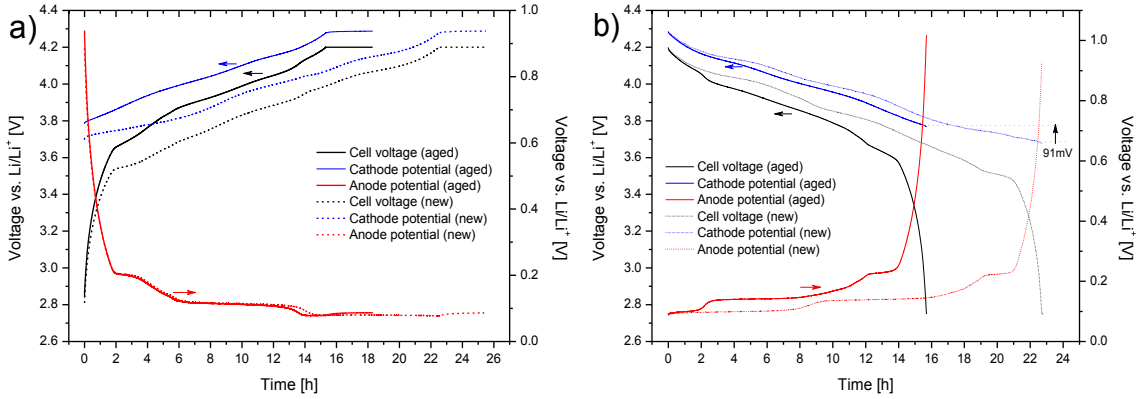

Fig. 5. Potential curves of new (dashed line) and aged (solid line) cell A, black curve: cell voltage of the complete cell A, blue curve: cathode potential of cell A, red curve: anode potential of cell A at a) charging and b) discharging. (For interpretation of the references to color in this figure legend, the reader is referred to the web version of this article.)

discharged state. The potential difference is charted in Fig. 5b and is 91 mV. On the other hand the cathode in the charged state is at the same potential, both for the new and for the aged cell. This is due to the fact that also in the aged state the anode is at the same potential than for the new anode, since the lowest plateau of the graphite is reached in both cases. Nevertheless it should be kept in mind that for a new anode in the charged state more lithium is intercalated in the graphite, whereas for the aged anode the lithium is captured in the SEI layer.

3.3. Materials analysis of the aged cell

The surface of the electrodes of cell A has been investigated by SEM and EDS analysis. Comparing new and aged cathodes at high magnifications (3000×) shows small differences in their visual appearance (Fig. 6). In the aged state cracks in the spinel particles appear as marked in Fig. 6b, which could be the reason for loss of active material (see Fig. 4 and Table 2). Besides that, cracking can also lead to a loose of electronic contact decreasing the battery performance.

Comparing the images in Fig. 6c and d shows SEM images of new and aged anode surfaces.

In Fig. 6d a distinct layer at the surface of the anode can be seen. This layer is composed possibly out of decomposition products of the electrolyte. A detailed description of a theory concerning this layer is given in a previous paper [16] and recent studies [20,5] At some positions the initial surface emerges beneath the surface layer. During disassembling of the cell A the separator has to be removed from the surface of the anode. In the aged state the separator sticks quite hard to the surface of the anode. It is not clear if parts of this surface layer stick to the separator and are thus detached unintended.

EDS analysis proved the presence of manganese is present at the aged anode surface. Dissolution of manganese can be caused by two main reaction mechanisms in the cell [17], which can be due to disproportionation of Mn^{3+} to Mn^{2+} and Mn^{4+} ions at low states of charge, or due to traces of HF within the electrolyte with $LiPF_6$. Because manganese ions do not change their oxidation state to Mn^{3+} during storage within the NMC and the spinel phase, manganese dissolution caused by HF is more likely. Dissolved transition metals are transported through the electrolyte to the surface of the anode and incorporate into the SEI layer [3,4,17,21] leading to an increased SEI layer growth. This causes loss of cycleable lithium, which is confirmed by the measurement shown in Fig. 5. Additionally the SEI layer is instable when exposed to elevated temperatures, which is another factor for continuous lithium consumption and thus capacity fade as the layer is continuously rebuild [22].

At this point the main aging mechanisms of the cell A can be summarized:

- The main reason for capacity fade of the cells is loss of cycleable lithium due to SEI layer growth. The growth of the SEI layer during aging is accelerated due to manganese dissolved from the cathode that it deposited on the anode.
- To a minor extent loss of positive active material coming from transition metal dissolution or isolated particles in the electrode [16] also accounts for capacity fade.
- The reason for the increase of the resistance of the cell is partially assigned to increase of the serial resistance, caused by a reduced electrolyte conductivity due to the consumption of salt during formation of the SEI and aging.

The following chapter will describe the influence of these aging phenomena on the safety of the aged cells to generate first cause–effect relations between aging and the thermal stability.

3.4. Thermal investigations

3.4.1. Complete lithium-ion cell

Fig. 7 shows the heating rate vs. temperature and the corresponding voltage vs. temperature profile of the ARC experiments of

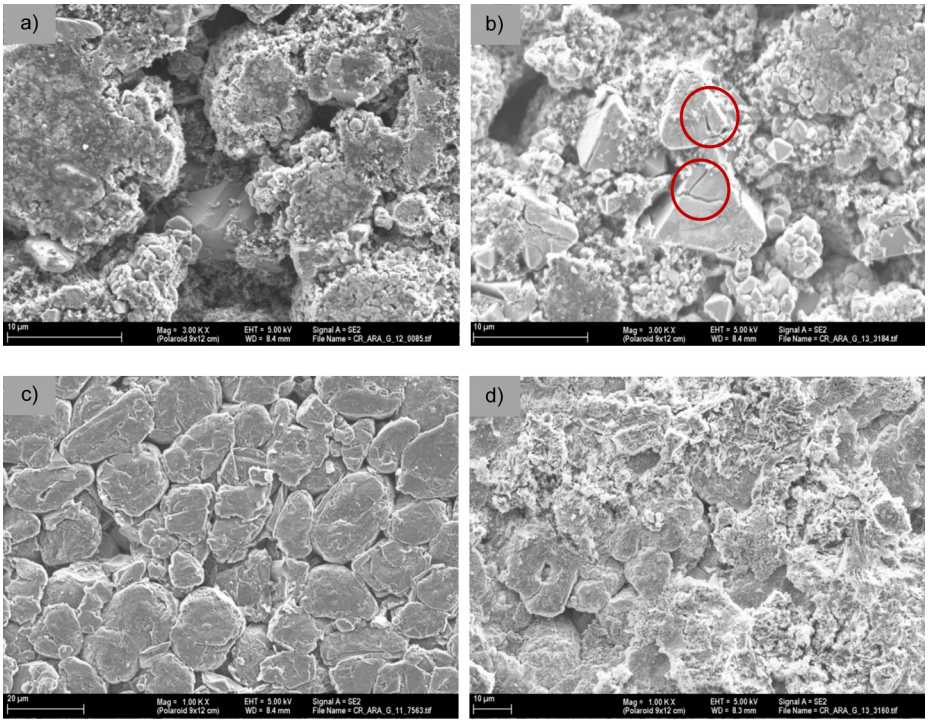

Fig. 6. Comparison of a) new cathode, b) 4.2 V (SOC100) calendar aged cathode, c) new anode and d) 4.2 V (SOC100) calendar aged anode of cell A at a magnification of 3000× and 1000×, respectively.

the complete lithium-ion cells both for a new and a calendar aged cell A at SOC100 and 60 °C for 36 weeks.

First of all, around 100 °C a significant rise in the voltage of both the new and the aged cell can be observed in Fig. 7a. We assume that this rise is caused by the shutdown effect of the separator of the cell (PP/PE/PP). Today, multilayer separators are used composed of at least two layers with different phase transition temperatures. When the melting point of the lower melting component is reached the pores are filled and ion transport in the cell is stopped. This means that at the shutdown point the cell becomes resistive and the voltage increases. Orendorff et al. [23] made the same observations, whereas, in his study the lithium-ion cell cooled down and a thermal runaway was prevented. In our case, both for the new and the aged cell a thermal runaway occurred with a respective onset-temperature of 105 °C for the aged and 110 °C for the new cell. At these temperatures a continuous rise of the self heating rate could be detected. Moreover, a heating rate of 1000 K min^{-1} was exceeded both for the new and the aged cell.

Regarding the thermal stability based on the ARC results there are two significant differences between the new and aged cell A which can be observed. Therefore, Fig. 8a shows the enlarged lower temperature range between 60 °C and 110 °C and Fig. 8b the corresponding enlarged upper temperature range between 100 °C and 300 °C.

In the lower temperature range it can be seen, that the new cell shows first exothermic signals around 90 °C. In contrast, the calendar aged cell A shows already around 70 °C first exothermic signals.

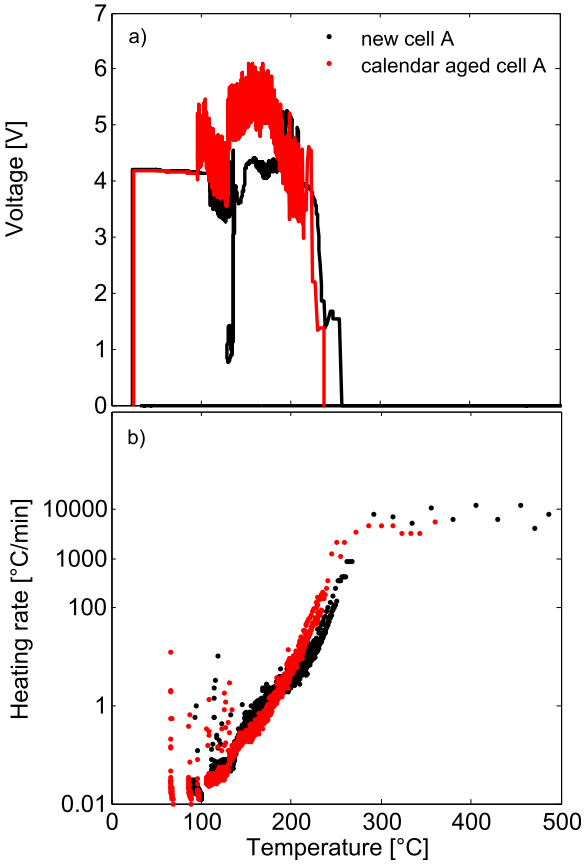

Fig. 7. a) Voltage vs. temperature profile (new and aged.) during the ARC test and b) heating rate vs. temperature plot (ARC) of the complete cell A (new and aged).

In the upper temperature domain the calendar aged cell A shows around 200 °C a slight steeper heating rate progress. Maleki et al. [12] showed that the reaction behavior of a complete lithium-ion cell in the lower temperature domain between 80 °C and 120 °C is dominated by reactions involving the anode. Especially the thermal decomposition behavior of the solid electrolyte interphase is decisive for the reaction behavior in this temperature range. The higher temperature range accompanied with a thermal runaway is dominated by the cathode- electrolyte reaction. Oxygen releases by a thermal induced decomposition of the cathode material and the oxidation with the organic based electrolyte are the dominant reactions [8,24]. Therefore, the thermal behavior of both the cathode and anode material of the cell A in contact with our reference electrolyte was investigated, respectively, by ARC and DSC to understand the thermal behavior of the complete lithium-ion cell from Figs. 7 and 8.

3.4.2. Thermal behavior of the anode

Fig. 9a shows the DSC results of the new and aged anode of cell A in contact with our reference electrolyte. The released heat values are also indicated in Fig. 9a.

First of all, we can observe a reduction of the main exothermic peak around 280 °C for the aged anode in contact with electrolyte compared to the reaction behavior of the new anode. The released heat is significantly reduced from 1544 J g^{-1} to 1144 J g^{-1}. Between 100 °C and 150 °C the DSC profile of the aged anode in contact with electrolyte shows a small exothermic signal, which could not be observed for the measurement with the new anode. In addition, Fig. 9a (inset figure) shows the corresponding enlarged temperature range between 100 °C and 150 °C.

The corresponding ARC measurements are shown in Fig. 9b. In this case, the same observations of the DSC measurements can be made for the ARC investigations.

Firstly, around 170 °C the main exothermic processes with a maximum heating rate around 1 K min^{-1} shows a reduced adiabatic temperature rise $\Delta T_{measured}$ for the aged anode ($\Delta T_{aged} < \Delta T_{new}$). According to Equation (3) this temperature rise is a measure for the released reaction heat ΔH.

$$\Delta H = m_{sample} \cdot c_{p,tot} \cdot \Delta T_{measured} \quad (3)$$

Secondly, the ARC measurement of the new anode the aged anode of cell A shows between an exothermic process between 80 °C and 100 °C. In contrast to the DSC measurement the processes are detected at lower temperatures. Depending on the scan rate, exothermic and endothermic processes are shifted to higher temperatures the higher the scan rate during a DSC experiment.

The decrease of the main exothermic process in the upper temperature range, which can be seen both in the DSC and ARC investigations, can be explained by the irreversible loss of cycleable lithium at the anode during calendar aging, therefore the aged anode contains a smaller amount of intercalated lithium in its charged state. This is already shown in Fig. 5. As consequence, the reaction behavior of the dominated reaction of lithium with electrolyte is significantly reduced.

The small exothermic signals detected both in the ARC (betweens 80 °C and 100 °C) and DSC (between 100 °C and 150 °C) investigations for the aged anode can be explained by the increased SEI. During calendar aging the SEI is damaged, e.g. by Mn dissolution, as described in Section 3.3 As consequence, intercalated lithium is consumed due to electrolyte reduction which leads to an increased SEI by deposition of reduction products. The passivating film could be observed in SEM analyses, shown in Fig. 6. In agreement with Spotnitz et al. [25] and MacNeil et al. [15], surface

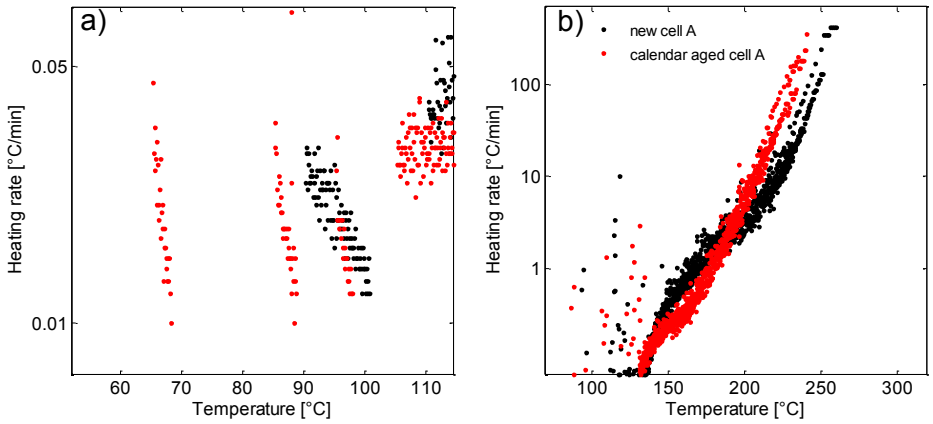

Fig. 8. Enlarged heating rate vs. temperature plot (ARC) from Fig. 7 of cell A b) between a) 60 °C and 110 °C and b) 100° and 300 °C.

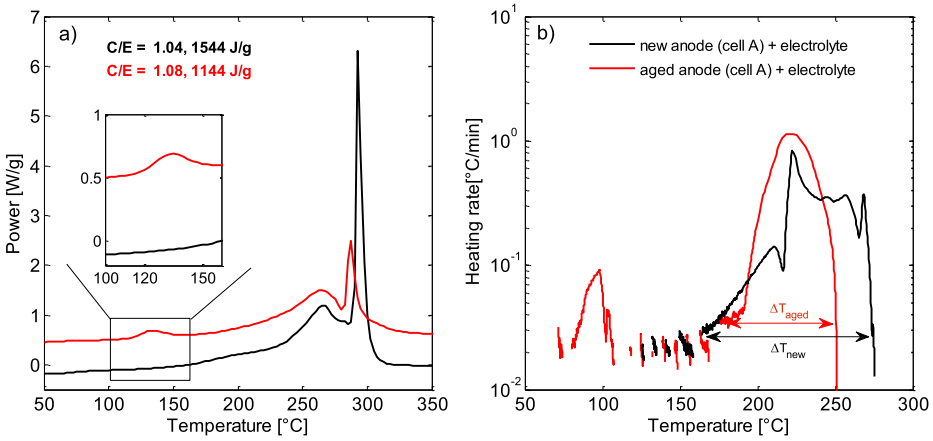

Fig. 9. a) DSC results of the new and aged anode of cell A in contact with electrolyte and b) heating rate vs. temperature plot (ARC) of the new and aged anode in contact with electrolyte.

processes including SEI reactions are taking place in the lower temperature range 80 °C–120 °C.

We suspect thereby, that the exothermic signals detected in case of the aged anode are clearly related to the reaction of the increased SEI with the electrolyte.

In addition, Fig. 10 shows the detected pressure rise of the new and aged anode of the cell A in contact with electrolyte. In case of the aged anode a significant exothermic pressure rise can be observed around 100 °C. According to [7], [26] and [27] the following reactions are taken into account generating exothermic behavior in the lower temperature range due to an increased SEI. A higher amount of inorganic components such as Li_2CO_3 [28] and organic components, like lithiumalkylcarbonates (ROCOOLi), are thereby expected.

$$LiPF_6 \leftrightarrows LiF + PF_5 \quad (4)$$

$$PF_5 + H_2O \rightarrow PF_3O + 2HF \quad (5)$$

$$ROCOOLi + HF \rightarrow ROCOOH + LiF \quad (6)$$

$$Li_2CO_3 + 2HF \rightarrow H_2O + CO_2 + 2LiF \quad (7)$$

Finally, the exothermic signal for the aged anode – electrolyte reaction detected both by ARC and DSC measurements in the lower temperature range can lead to the lower onset-temperature of the complete aged lithium-ion cell shown in Fig. 8a.

3.4.3. Thermal behavior of the cathode

As already described in the previous Section 3.4.1, the upper temperature domain (>150 °C) is dominated by the cathode-electrolyte reaction. The aged lithium-ion cell shows a slight

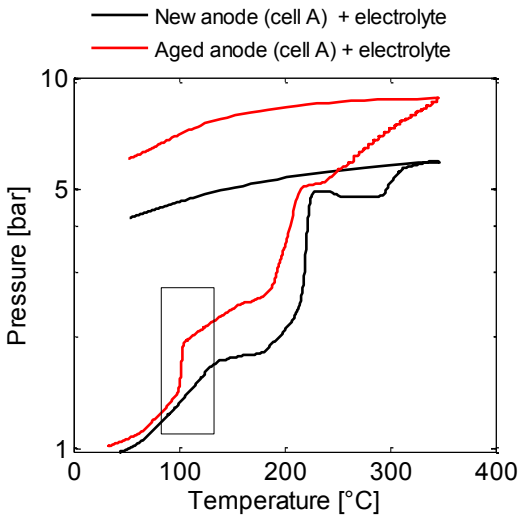

Fig. 10. Pressure vs. temperature plot (ARC) of the new and calendar aged anode of cell A in contact with electrolyte.

steeper heating rate development around 200 °C indicating a more violent reaction behavior (Fig. 8b). Comparable to the anode investigations, the cathode material of cell A was also studied by DSC and ARC, separately.

Fig. 11 a shows the corresponding DSC measurements. The exothermic peaks of the new and aged cathode show no significant deviation (black and red line). Also the released energy for both the new (784 J g^{-1}) and the aged (791 J g^{-1}) cathode in contact with electrolyte, respectively, shows no significant difference. Fig. 11b shows the corresponding ARC measurement of the new and aged cathode material in contact with electrolyte (black and red line).

Within the measurement accuracy, there is no significant deviation of the self heating rate between the new and the aged cathode material above 200 °C. In both cases a thermal runaway is observed around 260 °C. Moreover the total pressure rise of the new and aged cathode-electrolyte reaction, shown in Fig. 12, are also comparable.

Having regard to all the DSC and ARC results no significant decrease of the thermal stability of the aged cathode can be determined. The deviation of the heating rate in the upper temperature range of the complete lithium-ion cell (Figs. 7 and 8b) cannot be explained by our ARC and DSC investigations.

At this point is should be mentioned that the electrolyte added to the cathode or anode material was fresh. From disassembling of the lithium-ion cells (cell A and B) under argon atmosphere no electrolyte is available since it is nearly completely soaked in the pores of the electrodes and the separator. Therefore no aged electrolyte can be obtained from the cells. Up to now the influence of the aged electrolyte was neglected. Therefore, 1 ml of our reference electrolyte was aged at 60 °C in an aluminum vessel for 3 weeks. After that, the reaction behavior of the aged cathode in contact with our aged electrolyte was investigated by ARC and DSC. The results are shown in Fig. 11a and b (blue line). As first estimation, the reaction behavior by considering the released energy and the heating rate shows no significant difference. To study the influence of the aged electrolyte in detail further studies have to be done. As next step, a more realistic aging environment should be obtained. Therefore, the electrolyte could to be aged in contact with cathode material under the same conditions.

Both the electrochemical and the thermal stability of the cathode material depend on the potential of the cathode [29]. Thereby, the transition metals undergo oxidation to higher valences. A higher potential of the cathode decreases the intrinsic stability of the crystal and oxygen release can occur easier. As already described in Section 3.2, there is no rise of the aged cathode potential at SOC100 compared to the new (see Fig. 5). We assume thereby that the reaction behavior of the aged cathode is not significantly changed compared to the new cathode since the intrinsic stability determined by the potential state of the cathode is not changed.

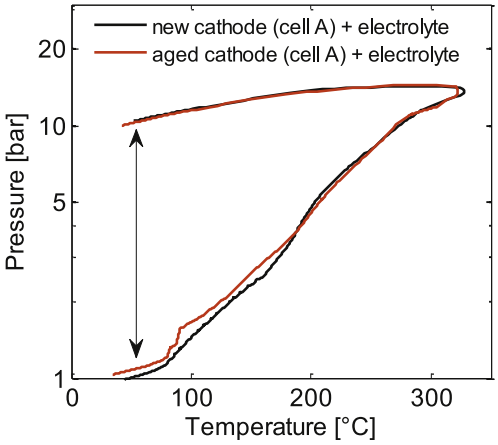

Fig. 12. Pressure vs. temperature plot (ARC) of the new and calendar aged cathode of cell A in contact with electrolyte.

After all, the ARC investigation of the complete aged cell shows a slight steeper heating rate progress compared to the new cell (see Fig. 8b). In Section 3.3 the SEM studies showed cracks in spinel particles which can lead to an increased surface area. Such an increased surface area can lead to a higher reactive surface area when oxygen is released from the cathode causing a more violent oxidation reaction. Such an effect was probably not detected during the ARC and DSC investigations since the cathode material has to be removed from the aluminum collector both for the new and the aged material. Due to this his preparation procedure the surface areas under coated conditions are no more present during measurement.

To investigate the effect of an increased cathode potential on the safety of an aged cell, a different cell-type (cell B) was used employing hard carbon at the anode, where a continuous potential change can be observed over the whole charging and discharging process. Hard carbon does not exhibit plateaus like graphite and thus forces the cathode to change its potential when the cell looses cycleable lithium.

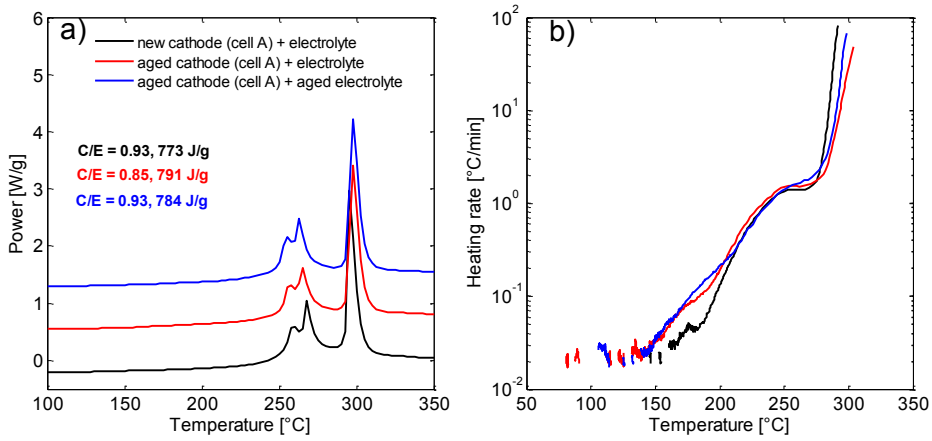

Fig. 11. a) DSC results of the new and aged cathode of cell A in contact with electrolyte and b) heating rate vs. temperature plot (ARC) of the new and aged cathode in contact with electrolyte. (For interpretation of the references to colour in this figure legend, the reader is referred to the web version of this article.)

Commercial hard carbon vs. NMC/LMO (4:1, w/w) based lithium-ion cells, labeled as cell B (2 Ah pouch-type), were calendar aged for 19 weeks at 60 °C at 4.2 V (SOC100). The capacity was determined every third week at a discharge rate of 1C. At the end of the calendar aging time the cell had a residual capacity of 1.5 Ah (1C − rate).

With the method, shown in Fig. 5, an increased cathode potential of 103 mV when fully charged was observed due to the continuous potential rise of hard carbon. Both on the complete lithium-ion cell B and the cathode material in contact with our reference electrolyte ARC measurements were carried out.

Fig. 13b shows the ARC experiment of the new and the calendar aged cell B. As expected, in the upper temperature domain a steeper self heating rate for the aged cell can be observed.

Fig. 14 shows the corresponding enlarged temperature domain. In contrast to Fig. 7 the steeper rise of the self heating rate is more significant. As already described, we assume that this is due the increased potential for the aged cathode resulting in a decreased intrinsic stability.

4. Conclusions

Within this study the aging phenomena during calendar aging at a defined aging condition at SOC100 and 60 °C of a commercial lithium-ion cell with a mixed $LiMn_2O_4$ (LMO)/$Li(Ni_{1/3}Mn_{1/3}Co_{1/3})O_2$ (NMC) cathode and a graphite anode were investigated by electrochemical and analytical tools. Using DSC and ARC, both on the cell level and on the material level, a change of the thermal behavior of the cell could be detected upon aging. The differences in the thermal behavior with respect to the new cell could be interpreted with the observed aging phenomena.

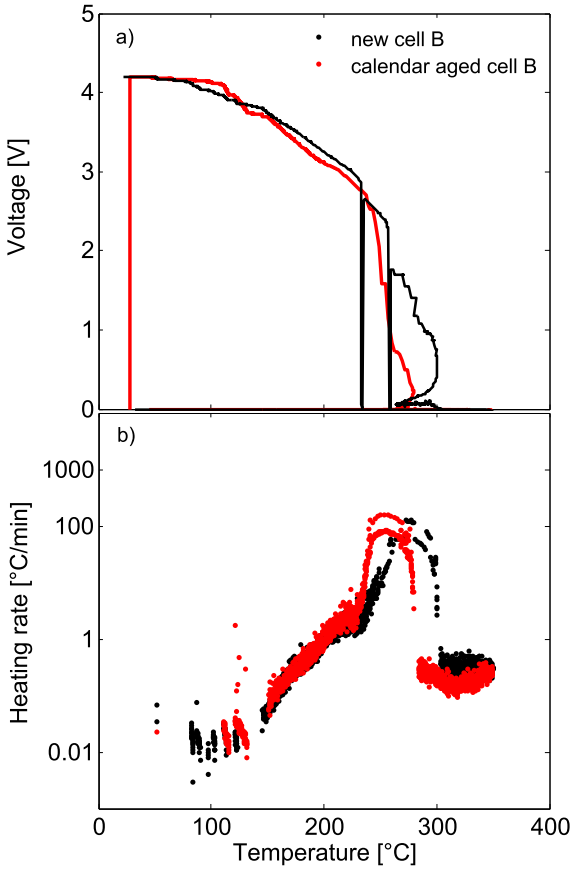

Fig. 13. a) Voltage vs. temperature profile (new and aged of cell B) during the ARC test and b) heating rate vs. temperature plot (ARC) of the complete hard carbon vs. NMC/LMO lithium-ion pouch 2 Ah − cell (new and aged).

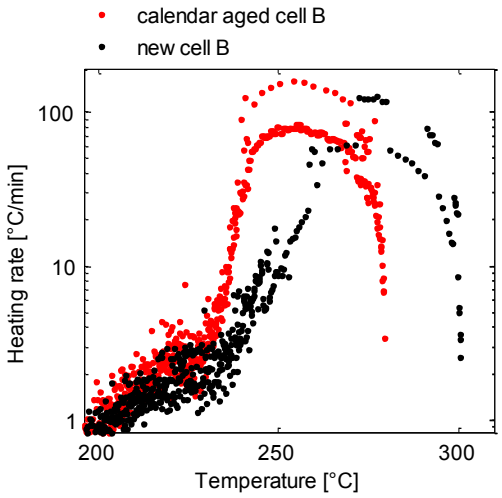

Fig. 14. Enlarged heating rate vs. temperature plot (ARC) from Fig. 13b) of cell B between 200 °C and 300 °C.

It was clearly shown that the main reason for capacity fade during calendar aging is the loss of cycleable lithium due to SEI layer growth. This could explain the thermal behavior of the electrodes in the aged state when compared with a fresh cell. Due to the more pronounced SEI layer in the aged state the onset-temperature is reduced, because more SEI layer is exothermically decomposed in the aged state. At the same time the overall energy released from the aged anode is significantly reduced. This is due to the fact that the aged anode in the charged state contains less intercalated lithium which could react with the electrolyte during the thermal investigations. On the other hand, the aged cathode/electrolyte reaction shows no significant deviation of its thermal behavior, since the potential of the aged cathode in the charged state has not changed. The slightly steeper heating rate for the aged lithium-ion cell above 200 °C can be ascribed to an increased surface area of the cathode. In the REM images of the aged cathode cracks in the LMO particles could be observed.

When using a hard carbon anode instead of a graphite anode the loss of cycleable lithium leads to an increase of the cathode potential in the charged state since the potential of the hard carbon anode changes continuously. As expected the charged cathode from an aged NMC/hard carbon cell shows a significantly steeper heating rate in the temperature range of cathode/electrolyte reactions. This effect can be ascribed to the increased cathode potential in the charged state.

To our knowledge there have been only very few studies in this area [13,30]. Most of the studies deal with fresh materials or with new cells only. Nevertheless, for use of lithium-ion batteries in automotive applications, it is important to guarantee safety in batteries for the entire lifetime, especially in aged cells. To understand the thermal behavior of an aged lithium-ion cell, cause–effect relationships between aging phenomena and the thermal behavior of the cell should be drawn, as shown in this study. Besides the aging condition exemplary considered in this work, it is also important to investigate further probable cause–effect relations for different aging conditions.

Acknowledgments

We gratefully acknowledge the funding of this work within the Linacore and alpha-Laion Project by the Federal Ministry of

Economy and Technology of Germany. The authors wish to thank the "Zentrum für Sonnenenergie- und Wasserstoff-Forschung" in Ulm for the ARC measurements of the complete lithium-ion cells.

References

[1] J. Belt, V. Utgikar, I. Bloom, J. Power Sources 196 (2011) 10213–10221.
[2] M. Winter, J. Besenhard, M. Spahr, P. Novák, Adv. Mater. 145 (1998) 725–763.
[3] P. Arora, R. White, M. Doyle, J. Electrochem. Soc. 145 (1998) 3647–3667.
[4] M. Wohlfahrts-Mehrens, C. Vogler, J. Garche, J. Power Sources 127 (2004) 58–64.
[5] M. Broussely, P. Biensan, F. Bonhomme, P. Blanchard, S. Herreyre, K. Nechev, R. Staniewicz, J. Power Sources 146 (2005) 90–96.
[6] Y. Wang, J. Jiang, J. Dahn, Electrochem. Commun. 9 (2007) 2434–2540.
[7] Q. Wang, P. Ping, J. Sun, C. Chen, Thermochim. Acta 517 (2011) 16–23.
[8] D. MacNeil, Z. Lu, Z. Chen, J. Dahn, J. Power Sources 108 (2002) 8–14.
[9] Z. Zhang, D. Fouchard, J. Rea, J. Power Sources 70 (1998) 16–20.
[10] S. Tobishima, K. Takei, Y. Sakurai, J. Yamaki, J. Power Sources 90 (2000) 188–195.
[11] S. Tobishima, J. Yamaki, J. Power Sources 81 (1999) 887–889.
[12] H. Maleki, J. Howard, J. Power Sources 137 (2004) 117–127.
[13] E. Roth, D. Doughty, J. Power Sources 12 (2004) 308–318.
[14] EL-Cell GmbH www.el-cell.com.
[15] D. MacNeil, J. Electrochem. Soc. 146 (1999) 3596.
[16] B. Stiaszny, J. Ziegler, E. Krauß, M. Zhang, J.P. Schmidt, E. Ivers-Tiffée, J. Power Sources 258 (2014) 61–75.
[17] J. Vetter, P. Novák, M. Wagner, C. Veit, K.-C. Möller, J. Besenhard, M. Winter, M. Wohlfahrt-Mehrens, C. Vogler, A. Hammouche, J. Power Sources 147 (2005) 269–281.
[18] N. Yabucchi, Y. Makimura, T. Ohzuku, J. Electrochem. Soc. 154 (2007) A314–A321.
[19] B. Stiaszny, J. Ziegler, E. Krauß, J.P. Schmidt, E. Ivers-Tiffée, J. Power Sources 251 (2014) 431–450.
[20] A. Zaban, D. Aurbach, J. Power Sources 54 (1995) 289–295.
[21] P. Ramadass, A. Durairajan, B. Haran, R. White, B. Popov, J. Electrochem. Soc. 149 (2002) A54–A60.
[22] T. Zheng, A. Gozdz, G. Amatucci, J. Electrochem. Soc. 146 (1999) 4014–4018.
[23] C. Orendorff, Electrochem. Soc. Interface Summer (2012).
[24] P. Röder, N. Baba, H. Wiemhöfer, J. Power Sources 248 (2014) 978–987.
[25] R. Spotnitz, J. Franklin, J. Power Sources 113 (2003) 81–100.
[26] D. Aurbach, J. Power Sources 89 (2000) 206.
[27] S. Sloop, J. Kerr, K. Kinoshita, J. Power Sources 119-121 (2003) 330–337.
[28] M. Richard, J. Dahn, J. Electrochem. Soc. 146 (1999) 2068–2077.
[29] R. Huggins, J. Electrochem. Soc. 160 (2013) A3001–A3005.
[30] M.-S. Wu, P.-C. Chiang, J.-C. Lin, Y. Jan, Electrochim. Acta 49 (2004) 1803–1812.